NANO LETTERS

pubs.acs.org/NanoLett Letter

The Buckling Spectra of Nanoparticle Surfactant Assemblies

Joe Forth, Andres Mariano, Yu Chai, Anju Toor, Jaffar Hasnain, Yufeng Jiang, Wenqian Feng, Xubo Liu, Phillip L. Geissler, Narayanan Menon, Brett A. Helms, Paul D. Ashby, and Thomas P. Russell*

Cite This: *Nano Lett.* 2021, 21, 7116–7122 Read Online

ACCESS | Metrics & More | Article Recommendations | Supporting Information

ABSTRACT: Fine control over the mechanical properties of thin sheets underpins transcytosis, cell shape, and morphogenesis. Applying these principles to artificial, liquid-based systems has led to reconfigurable materials for soft robotics, actuation, and chemical synthesis. However, progress is limited by a lack of synthetic two-dimensional membranes that exhibit tunable mechanical properties over a comparable range to that seen in nature. Here, we show that the bending modulus, B, of thin assemblies of nanoparticle surfactants (NPSs) at the oil−water interface can be varied continuously from sub-k_BT to 10^6 k_BT, by varying the ligands and particles that comprise the NPS. We find extensive departure from continuum behavior, including enormous mechanical anisotropy and a power law relation between B and the buckling spectrum width. Our findings provide a platform for shape-changing liquid devices and motivate new theories for the description of thin-film wrinkling.

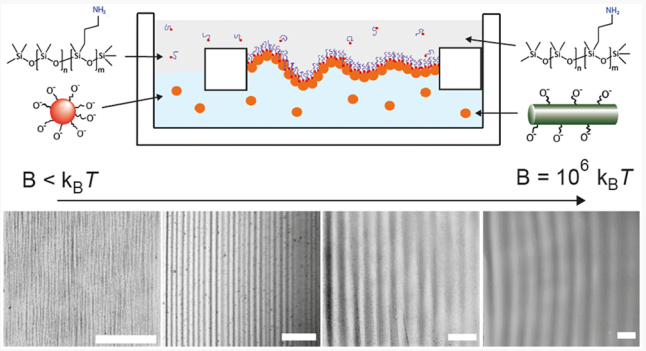

KEYWORDS: *Nanoparticles, wrinkling, self-assembly, interfaces, membranes*

Surface tension drives the assembly of nanoparticles (NPs) at liquid−liquid interfaces.[1] At sufficiently high densities, the NPs solidify into two-dimensional elastic sheets made of discrete building blocks.[2] These solid-like interfaces can be combined with additive manufacturing techniques to produce complex, hierarchical structures made entirely of liquids, such as bicontinuous networks,[3] fibrils,[4] and cellular materials.[5] Bringing this morphological control together with the enormous palette of functional nanomaterials that can now be synthesized has led to novel platforms for cell culture,[6] microfluidics,[7] and synthetic biology.[8] In these interface-rich materials, structure is determined by a balance between surface tension, adhesion energy, and the mechanical moduli of material assembled at the oil−water interface.[9] Fine control of these quantities inherently leads to shape control and actuation, allowing for the development of all-liquid, reconfigurable printed materials.[10] At the same time, dimensionally confined assemblies of NPs offer a system for testing the breakdown of continuum theories in nanoscale, granular, or high-aspect-ratio materials.[11] Critical to advancing both applied and fundamental aspects of these fields are interfacial nanoparticle assemblies whose mechanical properties can be readily tuned over orders of magnitude.[12,13]

Here, we study the bending moduli of assemblies of nanoparticle surfactants (NPSs) at the oil−water interface. NPSs consist of NPs and polymer surfactants that are initially dispersed in separate, immiscible liquids. Provided that the functional groups on the NPs and surfactants are complementary, e.g., ion pairing, the two components bind to one another at the liquid−liquid interface to form NPSs.[14] The resulting NPSs are irreversibly trapped at the interface, unless disassembled by an external stimulus. We used a Langmuir trough to study a silica nanoparticle-based NPS system whose adsorption kinetics and interfacial rheology we have extensively characterized elsewhere (Figure 1a).[15] The nonaqueous phase consisted of silicone oil (kinematic viscosity, 5 cSt) and NH_2-functionalized PDMS-based polymer surfactants (Figure 1b). Three different linear, amine-functionalized polymer surfactants were chosen that differ in their number of amine groups. PDMS-NH_2 has one terminal primary amine group, H_2N-PDMS-NH_2 is capped on both ends with primary amines, and an amine-functionalized random copolymer ("RCP") has multiple, randomly located amine groups per molecule. The aqueous phase contained 1 mg mL^{-1} of $-CO_2H$-functionalized spherical silica NPs (average radius 7 nm, polydispersity ≤10%, Figure 1c). A further system comprising rod-like, $-CO_2H$-functionalized cellulose nanocrystals (CNC, radius 5−10 nm, length 100−200 nm) in the aqueous phase and RCP (6 mM)

Received: April 13, 2021
Revised: August 20, 2021
Published: August 27, 2021

https://doi.org/10.1021/acs.nanolett.1c01454
Nano Lett. 2021, 21, 7116–7122

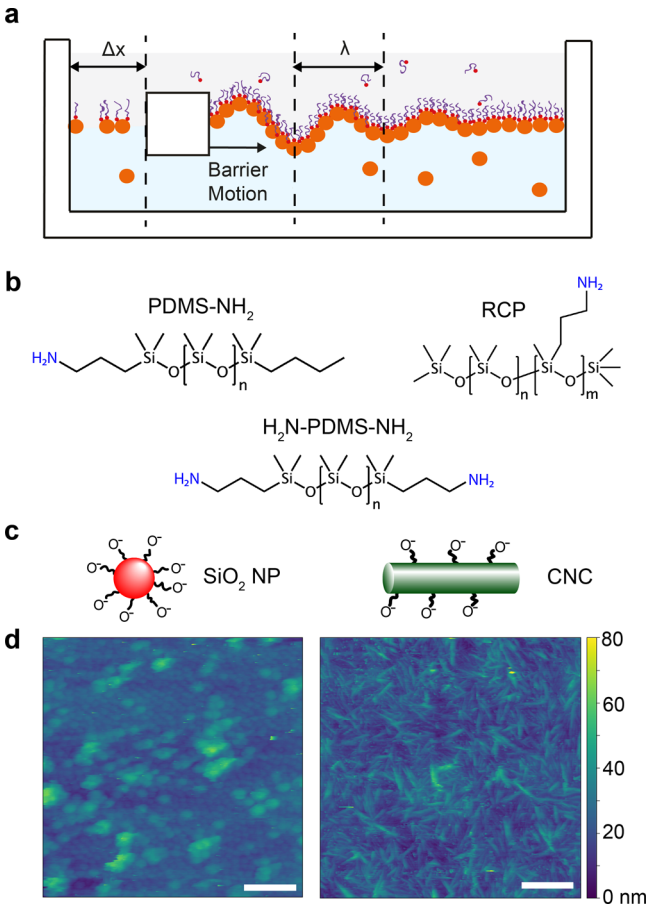

Figure 1. (a) Schematic of NPS formed at the oil−water interface in a Langmuir trough and the buckling of the assembly in response to confinement by a barrier. (b) NH_2-functionalized PDMS polymer surfactants dispersed in the nonaqueous phase. (c) CO_2H-functionalized silica nanoparticles and cellulose nanocrystals dispersed in the aqueous phase. (d) *In-situ* AFM height images of assemblies of 1 mg mL^{-1} SiO_2 NP with 20 mM H_2N-PDMS-NH_2 (scale bar, 100 nm) and 1 mg mL^{-1} CNC with 6 mM RCP (scale bar, 400 nm) at the oil−water interface.

in the nonaqueous phase was also studied, motivated by its use in all-liquid 3D printing and complementary AFM studies.[4,16]

The NPS assemblies were characterized *in situ* using liquid-phase atomic force microscopy (AFM) at the oil−water interface of an uncompressed, high-viscosity (kinematic viscosity, 60 000 cSt) silicone oil droplet (Figure 1d). In all but one case, AFM height images showed densely packed assemblies of discrete particles with short-range in-plane order, a narrow range of height variation smaller than a particle diameter (root-mean-square (RMS) roughness, 3−5 nm), and an absence of visible NPS in particle interstices, all of which are indicative of a monolayer (SI Figure 1). In one case (H_2N-PDMS-NH_2, 20 mM, SI Figure 1c) disordered assemblies with large-scale surface roughness (amplitude 50 nm, RMS roughness 13 nm) on an in-plane length scale of ∼100 nm were observed, indicative of aggregation of the particles and roughening of the assembly. After aging, extremely small translations of the barrier (of order microns) caused interfacial buckling and the formation of wrinkles in all cases. The wavelength of these wrinkles did not change on the experimental time scale and did not depend on the extent of barrier translation.

Translating the barriers of the trough led to the confinement of the NPSs and, hence, a spatially varying out-of-plane displacement of the assembly (Figure 2a−d; Videos S1−4 show representative data). The traditional, zero-temperature framework used to describe the shape adopted by the film in response to confinement considers the balance between the bending energy of the NPS assembly and the energetic cost of vertically displacing of the liquids.[17,18] This model predicts sinusoidal wrinkling patterns, in which a single, energetically favored wavelength, λ, of the wrinkles is related to the bending modulus, B, of the assembly as

$$\lambda = 2\pi\left(\frac{B}{\Delta\rho g}\right)^{1/4} \quad (1)$$

where $\Delta\rho$ is the density difference between the two liquid phases, and g = 9.8 m s^{-2}.

However, when confining our NPS assemblies, we did not see a single buckling wavelength, but rather an approximately Gaussian distribution of wavelengths (Figure 2e). The mean wavelength, $\bar{\lambda}$, which we treat as representing the bending modulus of the assembly, varied from ∼3 μm up to ∼300 μm, depending on the composition of the NPS studied. This translates to a range of B from sub-k_BT up to 10^6 k_BT (Figure 2f). The lowest B in SiO_2 NP-based systems was found when using RCP as a ligand, while the largest was ∼10^5 k_BT seen at the highest concentrations of H_2N-PDMS-NH_2, for which AFM topographs showed significant roughening of the interface. Larger still was the bending modulus of the CNC + RCP monolayers (∼10^6 k_BT).

Reproducibility between measurements was generally good, with most systems reproducing B to within around 50% of the mean. We attribute this variability to variations in functional group density on both NPs and polymer surfactants, as well as variation between batches in terms of particle diameter, molecular weight, and polydispersity. There was one notable exception: at 4 mM H_2N-PDMS-NH_2, an enormous spread in B was observed, from 10^2 k_BT up to 3 × 10^4 k_BT, suggesting that the significant roughening of the assembly seen in the AFM height images in Figure 1d occurs near this concentration. Wrinkling patterns at concentrations of RCP below 4.5 mM were either transient or highly variable and so not reported. Note that each data point in Figure 2f comprises measurements of wavelengths made at multiple different barrier translations for a single NPS film. This procedure was repeated for multiple films for each experimental condition, with each repeat yielding a single data point in Figure 2f (SI Figure 2).

Comparison with literature values is striking. NP assemblies at the liquid−fluid interface typically have extremely small mechanical moduli: Ag, Au, and Fe_3O_4 NP monolayers and trilayers spread at the liquid−air interface have a B of 10 k_BT or less.[19,20] By contrast, B as high as 10^7 k_BT has been reported in NP monolayers that have been processed into free-hanging assemblies or embedded in polymer matrices.[21,22] To our knowledge, the intermediate values for B in our NPS assemblies are not present in the literature. Measured B for lipid bilayers are typically in the range 10−100 k_BT,[23] while the reported lower bound for thin polymer films is typically on the order of 10^7−10^8 k_BT.[24] The judicious choice of ligands and particles in the NPS allow us control over B across this entire range.

https://doi.org/10.1021/acs.nanolett.1c01454
Nano Lett. 2021, 21, 7116−7122

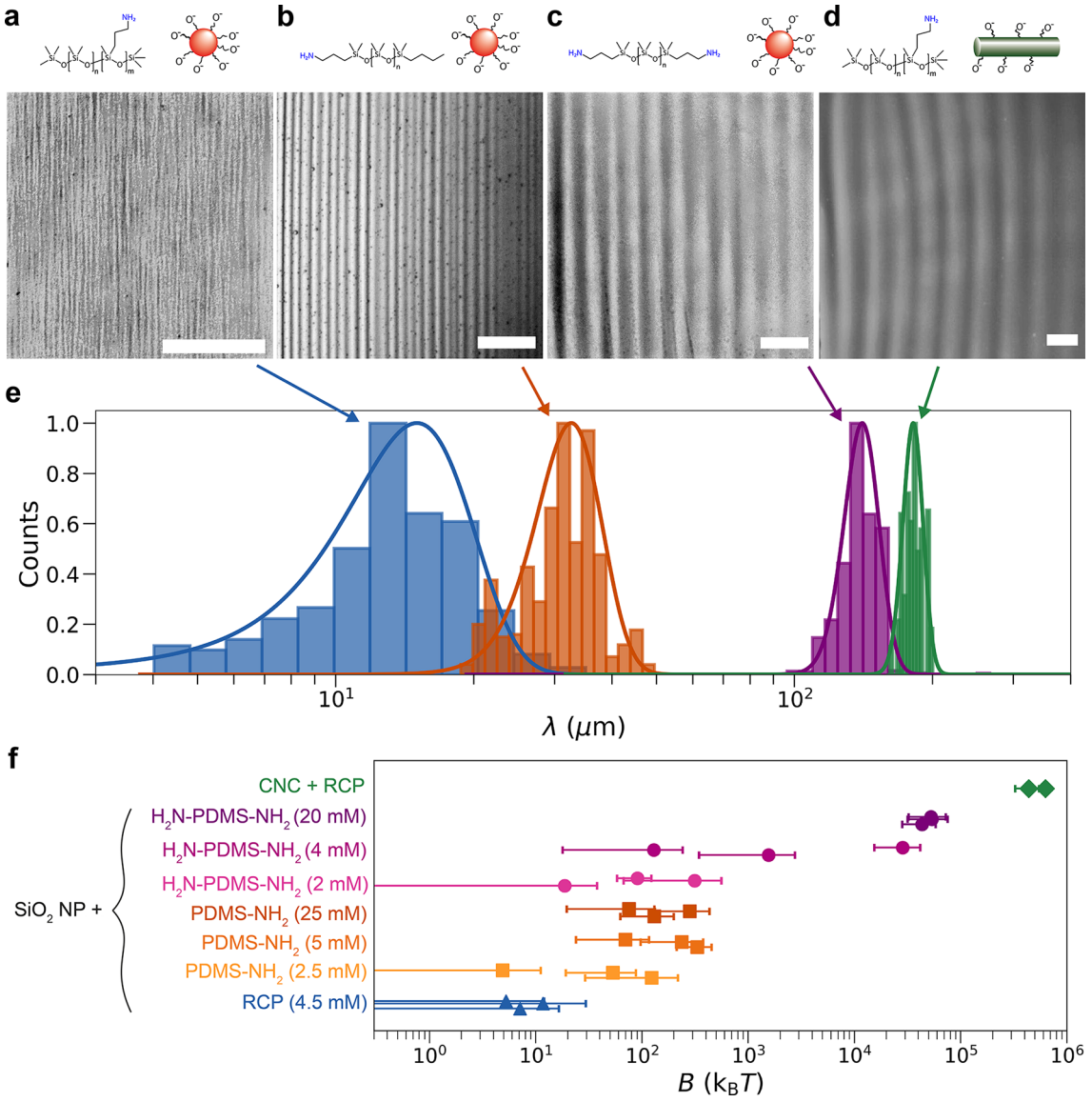

Figure 2. Wrinkles formed by confining NPS assemblies comprising SiO_2 NPs with (a) RCP (4.5 mM), (b) PDMS-NH_2 (25 mM), (c) H_2N-PDMS-NH_2 (20 mM), and (d) CNC with RCP (6 mM). Scale bars, 200 μm. (e) Normalized histograms of wrinkle wavelengths measured from different assemblies. Arrows indicate system composition, solid lines show Gaussian fits to the histograms. (f) Bending moduli for all systems studied in this work as inferred from buckling wavelengths. Each data point shows data obtained from a newly prepared NPS assembly. Error bars show ±1 standard deviation.

This variation in B stands in sharp contrast to the surface shear moduli, G_s, of the NPS assemblies (0.1−1 N m^{-1}),[15] demonstrating the enormous mechanical anisotropies of the NPS assemblies. Classical continuum relations predict that $B = \frac{G_s d^2}{6(1-\nu)}$, where ν is the Poisson ratio, overestimating the lower bound of our measured B by as much as 3 orders of magnitude. This anisotropy arises from the differing physical origins of the in-plane and out-of-plane mechanical response. Resistance to shear is due to the energetic costs of deforming the particle assembly at constant surface area.[25] By contrast, for out-of-plane deformations, the origins of B are less obvious. For the SiO_2 + H_2N-PDMS-NH_2 NPS, large B at high concentrations of polymer surfactant can be attributed to the roughening of the interface, leading to bulk-like mechanical properties. Capillary raft models, which predict that B derives from surface tension and the geometrical constraints placed on the oil−water interface, may be relevant for our assemblies with smaller bending modulus. These models predict B in the range 10^1−10^2 k_BT[26] and 10^1−10^5 k_BT[27], respectively, for SiO_2 NPS monolayers, which captures some of the range we see here, but not the phenomenology. Most importantly, both of these models predict an increase in B with surface tension; however, we find here that B either increases or is invariant with increasing polymer surfactant concentration (and, hence, decreasing surface tension).[15] Importantly, capillary raft models do not account for interactions between the polymer surfactants bound to our NPS, which are likely critical in our NPS, as they are asymmetrically coated by large (molecular weight of 2 kDa or more) polymer surfactants. Experimental studies have shown that ligand interactions significantly alter in-plane and out-of-plane mechanical properties of NP monolayers spread at the air−water interface.[20,28] However,

https://doi.org/10.1021/acs.nanolett.1c01454
Nano Lett. 2021, 21, 7116−7122

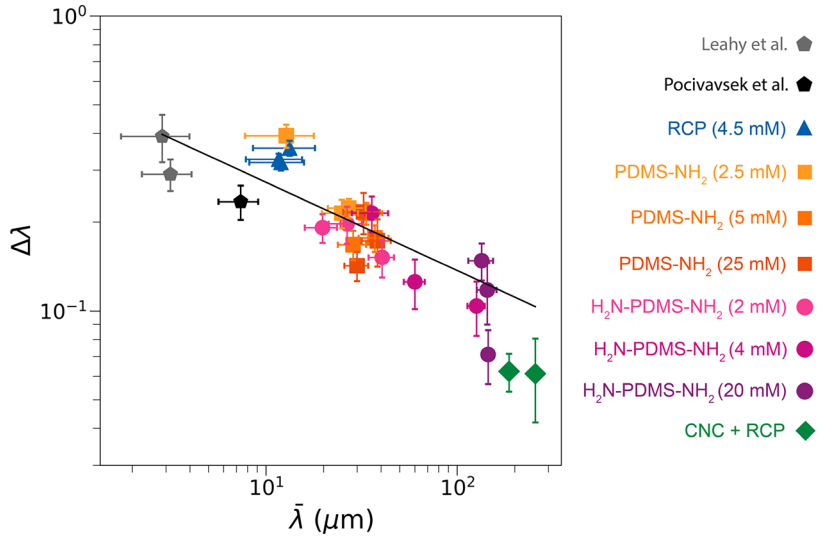

Figure 3. Power-law scaling of buckling spectrum width with buckling wavelength. Fit shows $\Delta\lambda = a\bar{\lambda}^{-b}$, with $a = 0.54$ and $b = 0.30$. Color scheme as in Figure 2; additional data series denoted in legend. Each data point shows an independent measurement. Error bars show ±1 standard deviation.

models allowing quantitative predictions of the effects of particle ligands on B are currently lacking in the literature.

The wide range in B we observe allows us to find further departure from classical buckling by studying the distribution of λ for a given B. Typical analyses of particle monolayer buckling predict the emergence of a single, energetically favorable mode in response to confinement. In the range of B studied in this work, however, approximately Gaussian distributions of wavelengths were seen (Figure 2e). As B decreases, the width of this distribution increases, and a broad spectrum of buckling modes emerges as B becomes comparable to thermal energies. Defining a buckling spectral width, $\Delta\lambda = \frac{\sigma_\lambda}{\bar{\lambda}}$, where σ_λ is the standard deviation of the measured distributions of wavelengths, it was found that $\Delta\lambda$ obeyed a power law relation with λ (Figure 3). Plotting $\Delta\lambda$ as a function of B (SI Figure 3) produces an identical trend. This relation is not a result of the palette of materials or solvents selected for our work. Even in samples where measurements of B varied significantly for each prepared assembly, such as 4 mM H_2N-PDMS-NH_2 + SiO_2 NP, each distinct measurement was found to lie on the trend line. Nor is the trend an artifact of imaging resolution: analysis of high-resolution data from Leahy et al.[19] (Au NPs spread at the air−water/ethanol and air/glycerol interface, $B < k_BT$), and Pocivavsek et al.[29] (Au NPs spread at the air−water interface, $B \approx k_BT$) produce spectral widths that fall onto the same trendline. This trend is not described by existing theories of thin film buckling. The classical theory of monolayer buckling at liquid−fluid interfaces of Milner et al. predicts buckling at a single wavelength.[17] By contrast, descriptions of fluctuating membranes predict that fluctuation amplitude will grow monotonically, reaching a maximum as the wavevector $\mathbf{q} \to 0$.[30] By contrast, our compressed monolayers buckle with a distribution of wavelengths that has a peak at nonzero wavevector and a width that broadens as B approaches thermal energies.

Finally, we comment on the confinement field in our trough, which exhibits qualitatively similar behavior independent of B (Figure 4). In all systems studied here, buckling is confined to within a few millimeters of the barrier that is being translated. Close to this barrier, stresses in the system are concentrated into highly curved folds. Moving away from the barrier, there exists a narrow region of length $\sim\lambda$, where the film transitions from folds to sinusoidal wrinkles. Beyond this, the amplitude of the wrinkles slowly decays (greater variations in gray value correspond to larger wrinkle amplitude). Far from the translating barrier, the assembly is planar. Both the decreasing amplitude of the wrinkles and the transition from folds to wrinkles, which occurs in response to increasing confinement, demonstrate that the effective degree of confinement of the film decays with increasing distance from the barrier.

This spatial decay in the degree of confinement is due to pinning of the NPS assembly at the edge of the trough. We confirmed this by imaging the CNC−RCP assembly (which had the largest λ) in dodecane, increasing the refractive index mismatch between the solvents and allowing us to obtain clear images of the system under reflection imaging without altering B (SI Figure 4). We clearly observed contact line pinning and large hysteresis effects at the edge of the trough upon reversing the applied confinement (Videos S5 and S6). It is important to note that the physical origin of these decays is different from that observed by Cicuta et al., which was attributed to frictional interactions of a spread monolayer of granular particles with the edges of the trough.[31] In our case, NPS assemblies form a network that spans the trough and are pinned at the wall of the trough. Conservatively taking the roughness of the wall, λ_r, to be of order 0.1−1.0 μm, we estimate that the three-phase contact line is pinned by capillary energies of order $\Delta E \sim \gamma\lambda_r^2 \approx 10^3$−$10^7$ k_BT, providing a significant barrier to relaxation of the folds into wrinkles.

Our results have their most immediate applications in microfluidics and reconfigurable, droplet-based materials. The enhanced bending moduli of the assemblies presented here are critical in balancing the overpressure produced by flows in all-liquid microfluidic platforms,[32] as well as in preventing structural failure due to Ostwald ripening.[33] In printed, droplet-based constructs, *in-situ* alteration of interfacial bending moduli could be used to drive shape changes and actuation.[34] Interfaces with tunable rigidity open the possibility of complex shape transformations in droplets containing synthetic cytoskeletons.[35] Finally, our findings motivate the

https://doi.org/10.1021/acs.nanolett.1c01454
Nano Lett. 2021, 21, 7116−7122

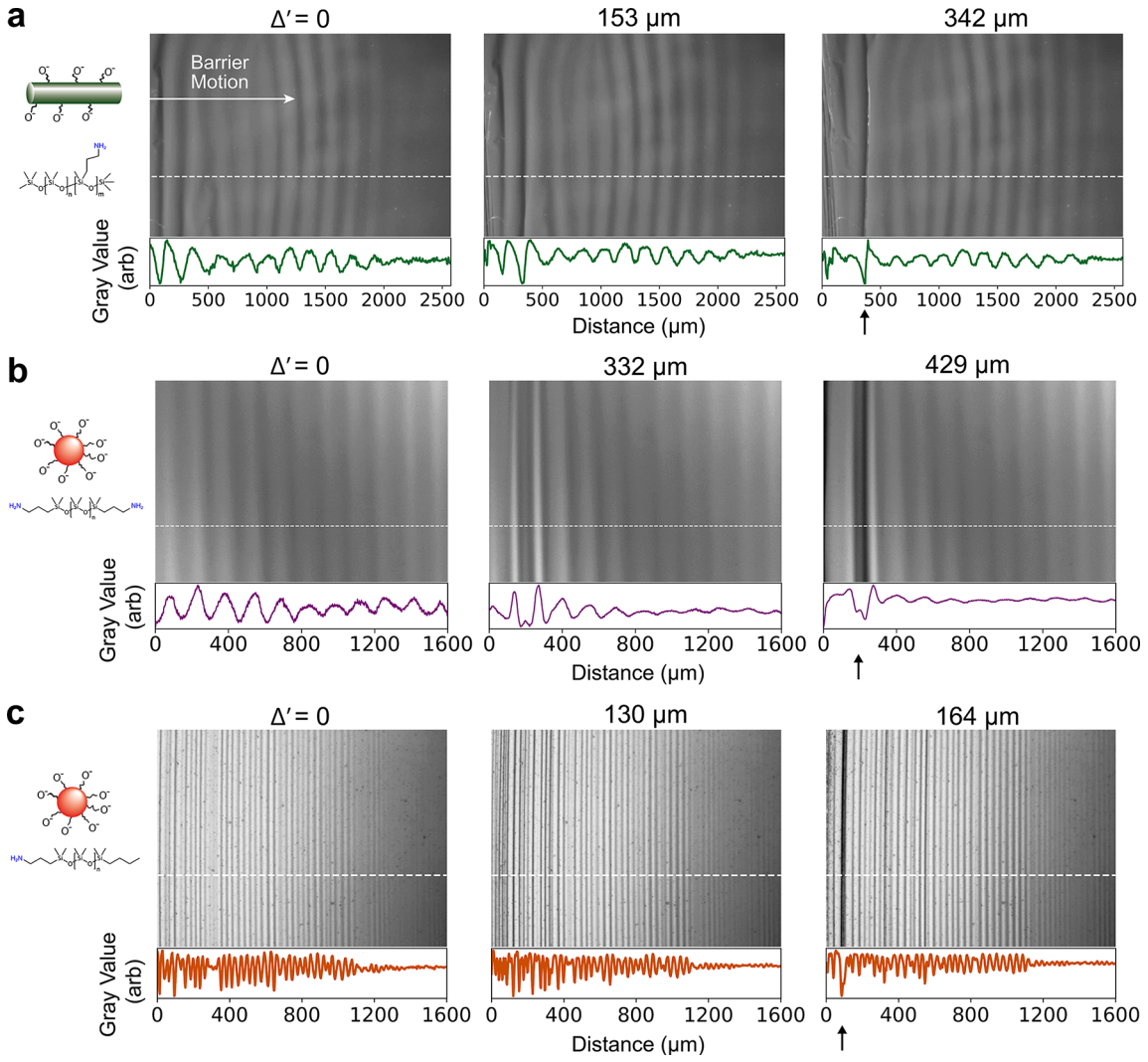

Figure 4. Coexistence of wrinkles and folds in NPS assemblies. Light micrographs of nanoparticle surfactant assemblies under increasing confinement, Δ′. Plots show gray-scale values after polynomial background subtraction. Note that the barrier was translated prior to experiment to produce wrinkles and Δ′ refers to further translations of the barrier. Gray-scale values measured in the region indicated by the white dashed line. Arrows indicate the location of a localized transition from a wrinkle to a fold. (a) 6 mM RCP, 1 mg mL^{-1} CNC. (b) 20 mM H_2N-PDMS-NH_2, 1 mg mL^{-1} SiO_2 NP. (c) 25 mM PDMS-NH_2, 1 mg mL^{-1} SiO_2 NP.

need for new theoretical tools that both account for the effects ligand–ligand interactions during NP monolayer buckling and describe the wrinkling of extremely thin materials made of discrete objects. Descriptions of homogeneous thin films buckling with multiple modes exist but do not capture the phenomena we observe here.[36] It may be that models that account for the discrete nature of the NPs are more successful in describing the mechanical properties of our assemblies.[37]

■ ASSOCIATED CONTENT

Supporting Information

The Supporting Information is available free of charge at https://pubs.acs.org/doi/10.1021/acs.nanolett.1c01454.

Materials and Methods and Figures S1–S4: AFM height images, bending moduli calculations, spectral width vs bending modulus, effect of solvent upon *B* (PDF)

Video S1: Compression of an NPS assembly. Aqueous phase contains 1 mg/mL cellulose nanocrystals. Nonaqueous is dodecane containing 6 mM amine-functionalized PDMS random copolymer. (MP4)

Video S2: Compression of an NPS assembly. Aqueous phase contains 1 mg/mL SiO_2 nanoparticles. Nonaqueous phase is 5 cSt silicone oil containing 20 mM H_2N-PDMS-NH_2. (MP4)

Video S3: Compression of an NPS assembly. Aqueous phase contains 1 mg/mL SiO_2 nanoparticles. Nonaqueous phase is 5 cSt silicone oil containing 25 mM PDMS-NH_2. (MP4)

Video S4: Compression of an NPS assembly. Aqueous phase contains 1 mg/mL SiO_2 nanoparticles. Nonaqueous phase is 5 cSt silicone oil containing 4.5 mM amine-functionalized PDMS random copolymer. (MP4)

Video S5: Compression of an NPS assembly showing pinning of the interfacial assembly at trough corners/edges. Aqueous phase contains 1 mg/mL cellulose nanocrystals. Nonaqueous phase is dodecane containing 6 mM amine-functionalized PDMS random copolymer. (MP4)

Video S6: Retraction of barrier after confinement of NPS assembly showing pinning of the interfacial

https://doi.org/10.1021/acs.nanolett.1c01454
Nano Lett. 2021, 21, 7116–7122

assembly at trough corners/edges. Aqueous phase contains 1 mg/mL cellulose nanocrystals. Nonaqueous phase is dodecane containing 6 mM amine-functionalized PDMS random copolymer. (MP4)

AUTHOR INFORMATION

Corresponding Author

Thomas P. Russell − *Materials Sciences Division, Lawrence Berkeley National Laboratory, Berkeley, California 94720, United States; Polymer Science and Engineering Department, University of Massachusetts, Amherst, Massachusetts 01003, United States; Beijing Advanced Innovation Center for Soft Matter Science and Engineering, Beijing University of Chemical Technology, Beijing 100029, China; Advanced Institute for Materials Research (WPI-AIMR), Tohoku University, Aoba, Sendai 980-8577, Japan;* orcid.org/0000-0001-6384-5826; Email: tom.p.russell@gmail.com

Authors

Joe Forth − *Materials Sciences Division, Lawrence Berkeley National Laboratory, Berkeley, California 94720, United States; Department of Chemistry, University College London, London WC1H 0AJ, United Kingdom;* orcid.org/0000-0001-7263-6364

Andres Mariano − *Materials Sciences Division, Lawrence Berkeley National Laboratory, Berkeley, California 94720, United States; Department of Chemistry, University of California, Berkeley, California 94720, United States*

Yu Chai − *Materials Sciences Division, Lawrence Berkeley National Laboratory, Berkeley, California 94720, United States; Molecular Foundry, Lawrence Berkeley National Laboratory, Berkeley, California 94720, United States; Department of Physics, City University of Hong Kong, Hong Kong, SAR, China;* orcid.org/0000-0001-6085-4321

Anju Toor − *Materials Sciences Division, Lawrence Berkeley National Laboratory, Berkeley, California 94720, United States; School of Materials Science and Engineering, University of California, Berkeley, California 94720, United States*

Jaffar Hasnain − *Materials Sciences Division, Lawrence Berkeley National Laboratory, Berkeley, California 94720, United States; Department of Chemistry, University of California, Berkeley, California 94720, United States*

Yufeng Jiang − *Materials Sciences Division, Lawrence Berkeley National Laboratory, Berkeley, California 94720, United States; School of Materials Science and Engineering, University of California, Berkeley, California 94720, United States*

Wenqian Feng − *Materials Sciences Division, Lawrence Berkeley National Laboratory, Berkeley, California 94720, United States*

Xubo Liu − *Materials Sciences Division, Lawrence Berkeley National Laboratory, Berkeley, California 94720, United States; Beijing Advanced Innovation Center for Soft Matter Science and Engineering, Beijing University of Chemical Technology, Beijing 100029, China*

Phillip L. Geissler − *Materials Sciences Division, Lawrence Berkeley National Laboratory, Berkeley, California 94720, United States; Department of Chemistry, University of California, Berkeley, California 94720, United States;* orcid.org/0000-0003-0268-6547

Narayanan Menon − *Department of Physics, University of Massachusetts, Amherst, Massachusetts 01003, United States*

Brett A. Helms − *Materials Sciences Division, Lawrence Berkeley National Laboratory, Berkeley, California 94720, United States; Molecular Foundry, Lawrence Berkeley National Laboratory, Berkeley, California 94720, United States;* orcid.org/0000-0003-3925-4174

Paul D. Ashby − *Materials Sciences Division, Lawrence Berkeley National Laboratory, Berkeley, California 94720, United States; Molecular Foundry, Lawrence Berkeley National Laboratory, Berkeley, California 94720, United States;* orcid.org/0000-0003-4195-310X

Complete contact information is available at: https://pubs.acs.org/10.1021/acs.nanolett.1c01454

Funding

This work was supported by the U.S. Department of Energy, Office of Science, Office of Basic Energy Sciences, Materials Sciences and Engineering Division under Contract No. DE-AC02−05-CH11231 within the Adaptive Interfacial Assemblies Toward Structuring Liquids program (KCTR16). Portions of the work—including the AFM imaging—were carried out as a User Project at the Molecular Foundry, which is supported under the same contract. J.F. was supported by a Ramsay Memorial Fellowship during the preparation of the manuscript.

Notes

The authors declare no competing financial interest.

REFERENCES

(1) Dong, A.; Chen, J.; Vora, P. M.; Kikkawa, J. M.; Murray, C. B. Binary Nanocrystal Superlattice Membranes Self-Assembled at the Liquid-Air Interface. *Nature* **2010**, *466* (7305), 474−477.

(2) Stratford, K.; Adhikari, R.; Pagonabarraga, I.; Desplat, J.-C.; Cates, M. E. Colloidal Jamming at Interfaces: A Route to Fluid-Bicontinuous Gels. *Science* **2005**, *309*, 2198−2201.

(3) Herzig, E. M.; White, K. A.; Schofield, A. B.; Poon, W. C. K.; Clegg, P. S. Bicontinuous Emulsions Stabilized Solely by Colloidal Particles. *Nat. Mater.* **2007**, *6*, 966−971.

(4) Forth, J.; Liu, X.; Hasnain, J.; Toor, A.; Miszta, K.; Shi, S.; Geissler, P. L.; Emrick, T.; Helms, B. A.; Russell, T. P. Reconfigurable Printed Liquids. *Adv. Mater.* **2018**, *30* (16), 1707603.

(5) Villar, G.; Heron, A. J.; Bayley, H. Formation of Droplet Networks That Function in Aqueous Environments. *Nat. Nanotechnol.* **2011**, *6* (12), 803−808.

(6) Zhou, L.; Wolfes, A. C.; Li, Y.; Chan, D. C. W.; Ko, H.; Szele, F. G.; Bayley, H. Lipid-Bilayer-Supported 3D Printing of Human Cerebral Cortex Cells Reveals Developmental Interactions. *Adv. Mater.* **2020**, *32* (31), 2002183.

(7) Feng, W.; Chai, Y.; Forth, J.; Ashby, P. D.; Russell, T. P.; Helms, B. A. Harnessing Liquid-in-Liquid Printing and Micropatterned Substrates to Fabricate 3-Dimensional All-Liquid Fluidic Devices. *Nat. Commun.* **2019**, *10* (1), 1095.

(8) Rodríguez-Arco, L.; Li, M.; Mann, S. Phagocytosis-Inspired Behaviour in Synthetic Protocell Communities of Compartmentalized Colloidal Objects. *Nat. Mater.* **2017**, *16* (8), 857−863.

(9) Alt, S.; Ganguly, P.; Salbreux, G. Vertex Models: From Cell Mechanics to Tissue Morphogenesis. *Philos. Trans. R. Soc., B* **2017**, *372* (1720), 20150520.

(10) Villar, G.; Graham, A. D.; Bayley, H. A Tissue-Like Printed Material. *Science (Washington, DC, U. S.)* **2013**, *340*, 48−52.

(11) Davidovitch, B.; Schroll, R. D.; Vella, D.; Adda-Bedia, M.; Cerda, E. a. Prototypical Model for Tensional Wrinkling in Thin Sheets. *Proc. Natl. Acad. Sci. U. S. A.* **2011**, *108* (45), 18227−18232.

(12) Yang, Z.; Wei, J.; Sobolev, Y. I.; Grzybowski, B. A. Systems of Mechanized and Reactive Droplets Powered by Multi-Responsive Surfactants. *Nature* **2018**, *553*, 313−318.

(13) Forth, J.; Kim, P. Y.; Xie, G.; Liu, X.; Helms, B. A.; Russell, T. P. Building Reconfigurable Devices Using Complex Liquid−Fluid Interfaces. *Adv. Mater.* **2019**, *31*, 1806370.
(14) Cui, M.; Emrick, T.; Russell, T. P. Stabilizing Liquid Drops in Nonequilibrium Shapes by the Interfacial Jamming of Nanoparticles. *Science (Washington, DC, U. S.)* **2013**, *342* (6157), 460−464.
(15) Toor, A.; Forth, J.; Bochner de Araujo, S.; Merola, M. C.; Jiang, Y.; Liu, X.; Chai, Y.; Hou, H.; Ashby, P. D.; Fuller, G. G.; Russell, T. P. Mechanical Properties of Solidifying Assemblies of Nanoparticle Surfactants at the Oil−Water Interface. *Langmuir* **2019**, *35*, 13340−13350.
(16) Wu, X.; Yuan, Q.; Liu, S.; Shi, S.; Russell, T. P.; Wang, D. Nanorod−surfactant Assemblies and Their Interfacial Behavior at Liquid−liquid Interfaces. *ACS Macro Lett.* **2019**, *8* (5), 512−518.
(17) Milner, S. T.; Joanny, J.-F.; Pincus, P. Buckling of Langmuir Monolayers. *Europhys. Lett.* **1989**, *9*, 495−500.
(18) Zhang, Q.; Witten, T. A. Microscopic Wrinkles on Supported Surfactant Monolayers. *Phys. Rev. E - Stat. Nonlinear, Soft Matter Phys.* **2007**, *76* (4), 1−11.
(19) Leahy, B. D.; Pocivavsek, L.; Meron, M.; Lam, K. L.; Salas, D.; Viccaro, P. J.; Lee, K. Y. C.; Lin, B. Geometric Stability and Elastic Response of a Supported Nanoparticle Film. *Phys. Rev. Lett.* **2010**, *105*, 1 DOI: 10.1103/PhysRevLett.105.058301.
(20) You, S. S.; Rashkov, R.; Kanjanaboos, P.; Calderon, I.; Meron, M.; Jaeger, H. M.; Lin, B. Comparison of the Mechanical Properties of Self-Assembled Langmuir Monolayers of Nanoparticles and Phospholipids. *Langmuir* **2013**, *29* (37), 11751−11757.
(21) Mueggenburg, K. E.; Lin, X.-M.; Goldsmith, R. H.; Jaeger, H. M. Elastic Membranes of Close-Packed Nanoparticle Arrays. *Nat. Mater.* **2007**, *6* (9), 656−660.
(22) Gu, X. W.; Ye, X.; Koshy, D. M.; Vachhani, S.; Hosemann, P.; Alivisatos, A. P. Tolerance to Structural Disorder and Tunable Mechanical Behavior in Self-Assembled Superlattices of Polymer-Grafted Nanocrystals. *Proc. Natl. Acad. Sci. U. S. A.* **2017**, *114* (11), 2836−2841.
(23) Elani, Y.; Purushothaman, S.; Booth, P. J.; Seddon, J. M.; Brooks, N. J.; Law, R. V.; Ces, O. Measurements of the Effect of Membrane Asymmetry on the Mechanical Properties of Lipid Bilayers. *Chem. Commun.* **2015**, *51* (32), 6976−6979.
(24) Huang, J.; Davidovitch, B.; Santangelo, C. D.; Russell, T. P.; Menon, N. Smooth Cascade of Wrinkles at the Edge of a Floating Elastic Film. *Phys. Rev. Lett.* **2010**, *105* (3), 2−5.
(25) Maestro, A.; Zaccone, A. Nonaffine Deformation and Tunable Yielding of Colloidal Assemblies at the Air−Water Interface. *Nanoscale* **2017**, *9* (46), 18343−18351.
(26) Vella, D.; Aussillous, P.; Mahadevan, L. Elasticity of an Interfacial Particle Raft. *Europhys. Lett.* **2004**, *68*, 212−218.
(27) Kralchevsky, P. A.; Ivanov, I. B.; Ananthapadmanabhan, K. P.; Lips, A. On the Thermodynamics of Particle-Stabilized Emulsions: Curvature Effects and Catastrophic Phase Inversion. *Langmuir* **2005**, *21* (1), 50−63.
(28) Griesemer, S. D.; You, S. S.; Kanjanaboos, P.; Calabro, M.; Jaeger, H. M.; Rice, S. A.; Lin, B. The Role of Ligands in the Mechanical Properties of Langmuir Nanoparticle Films. *Soft Matter* **2017**, *13* (17), 3125−3133.
(29) Pocivavsek, L.; Dellsy, R.; Kern, A.; Johnson, S.; Lin, B.; Lee, K. Y. C.; Cerda, E. Stress and Fold Localization in Thin Elastic Membranes. *Science (Washington, DC, U. S.)* **2008**, *320*, 912−916.
(30) Safran, S. A. *Statistical Thermodynamics of Surfaces, Interfaces, and Membranes*; CRC Press, 2003.
(31) Cicuta, P.; Vella, D. Granular Character of Particle Rafts. *Phys. Rev. Lett.* **2009**, *102* (13), 1−4.
(32) Di Vitantonio, G.; Wang, T.; Haase, M. F.; Stebe, K. J.; Lee, D. Robust Bijels for Reactive Separation via Silica-Reinforced Nanoparticle Layers. *ACS Nano* **2019**, *13*, 26−31.
(33) Abkarian, M.; Subramaniam, A. B.; Kim, S. H.; Larsen, R. J.; Yang, S. M.; Stone, H. A. Dissolution Arrest and Stability of Particle-Covered Bubbles. *Phys. Rev. Lett.* **2007**, *99* (18), 1−4.
(34) Santa Chalarca, C. F.; Letteri, R. A.; Perazzo, A.; Stone, H. A.; Emrick, T. Building Supracolloidal Fibers from Zwitterion-Stabilized Adhesive Emulsions. *Adv. Funct. Mater.* **2018**, *28* (45), 1−10.
(35) Caggioni, M.; Lenis, J.; Bayles, A. V.; Furst, E. M.; Spicer, P. T. Temperature-Induced Collapse, and Arrested Collapse, of Anisotropic Endoskeleton Droplets. *Langmuir* **2015**, *31* (31), 8558−8565.
(36) Matoz-Fernandez, D. A.; Davidson, F. A.; Stanley-Wall, N. R.; Sknepnek, R. Wrinkle Patterns in Active Viscoelastic Thin Sheets. *Phys. Rev. Res.* **2020**, *2*, 013165.
(37) Tordesillas, A.; Carey, D.; Croll, A. B.; Shi, J.; Gurmessa, B. Micromechanics of Elastic Buckling of a Colloidal Polymer Layer on a Soft Substrate: Experiment and Theory. *Granular Matter* **2014**, *16* (2), 249−258.

https://doi.org/10.1021/acs.nanolett.1c01454
Nano Lett. 2021, 21, 7116−7122